International Journal of Marine Science and Technology, vol. 1, no.1, pp.8–16, 2025 e-ISSN: 3093-3609
https://doi.org/10.65154/ijmst.11 https://i-jmst.vimaru.edu.vn

A Study of Stress-Strain Relationships of Longitudinal Structural Elements of Bulk Carriers under Vertical Bending Moment

Van Tuyen Vu*, Quang Quan Do, Huy Chinh Cu, and Huy Vu Nguyen

Abstract: The paper evaluates the stress-strain relationships of different structural element groups of ship structures subjected to longitudinal bending moments at the ultimate limit state (ULS). The incremental-iterative method proposed by the International Association of Classification Societies (IACS) is applied. In this method, the hull cross-section is divided into three groups of structural elements, each assigned to one of six common failure modes. Bulk carriers (BCs) are employed to illustrate the calculation results. Accordingly, the paper presents the stress-strain curves of the different structural element groups, as well as the stress and strain experienced by each structural element at the ULS under hogging and sagging conditions. One notable finding is that the sagging condition generates higher stresses in the ship structure compared to the hogging condition. The top-side tank region experiences the highest stress levels, reaching the material's yield stress when the ship approaches its ultimate longitudinal bending capacity. Additional discussions are also provided in this paper.

Keywords: Bending moments, limit state, stress-strain relationship, structural element, incremental-iterative method.

1. INTRODUCTION

When subjected to hull-girder loading, the structural capacity of the hull may approach its ULS, where significant variations in structural behavior occur. Among several parameters, axial stresses and strains are primary indicators for assessing the ultimate strength (US) of individual structural elements, and understanding their behavior is essential for evaluating the global ULS of the hull girder. Previous related studies can be summarized as follows.

For unstiffened plates, Sultana et al. [1] used numerical analyses to examine the influence of slenderness ratio, plate thickness, aspect ratio, and pitting characteristics on the strength of stiffened and unstiffened panels, presenting both average and normalized stress-strain curves. The tensile performance of 51 corroded steel specimens was evaluated through finite elememt analysis (FEA) and tensile testing, focusing on deformation, stress-strain relationships, load-strength behavior, minimum section area, stress distribution, and stress concentration factors [2]. He and Soares [3] investigated the dynamic responses of rectangular mild-steel plates using numerical and experimental approaches. Shiomitsu et al. [4] applied nonlinear finite element analysis (NFEA), considering buckling and post-buckling behavior, initial imperfections, material properties, and geometric ratios, to propose simplified estimates of biaxial and shear US for rectangular plates.

For stiffened plates, corrosion wastage has been widely studied. Randomly distributed corrosion and variable thickness were used to examine their influence on the strength and collapse behavior of stiffened panels [5]. Additional studies assessed the effects of general corrosion, material properties, lateral pressure, initial imperfections, and biaxial compression on the ULS of stiffened panels from four common tanker types [6]. The effects of pitting corrosion, including degree of pitting (DOP), depth, location, and distribution on strength reduction, stress-strain behavior, and deformation were examined for three panel types [7]. Other research focused on geometric effects: Hacihamud et al. [8] investigated geometric nonlinearities, stiffener-span imperfections, span length, and holes on buckling under uniaxial loading; and Hanif et al. [9] studied ULS and collapse behavior under varying model configurations, boundary conditions, and stiffener models, summarizing stress-strain and von Mises responses. Kim et al. [10] performed extensive NFEA on 124 stiffened panels to

Manuscript received October 28, 2025; received in revised form November 17, 2025; accepted December 08, 2025; available online December 30, 2025.

Van Tuyen Vu, Quang Quan Do, and Huy Chinh Cu are with the Faculty of Shipbuilding, Vietnam Maritime University, Haiphong, Vietnam (e-mails: tuyenvv.dt@vimaru.edu.vn, quandq.dt@vimaru.edu.vn, and chinhch.dt@vimaru.edu.vn). Huy Vu Nguyen is with the Department of Systems Engineering and Naval Architecture, National Taiwan Ocean University, Keelung 20224, Taiwan (e-mail: vunh@ntu.edu.vn).
* Corresponding author.

Research article

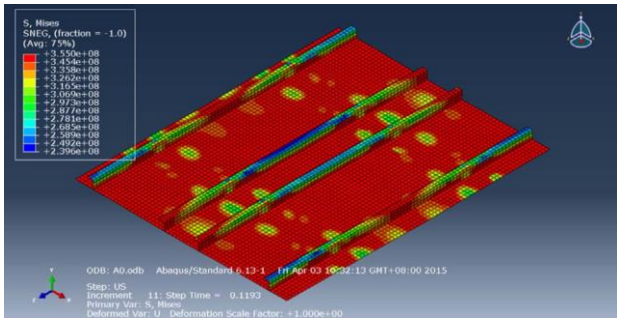

Fig. 1. Stress distribution and displacements at ultimate strength [13].

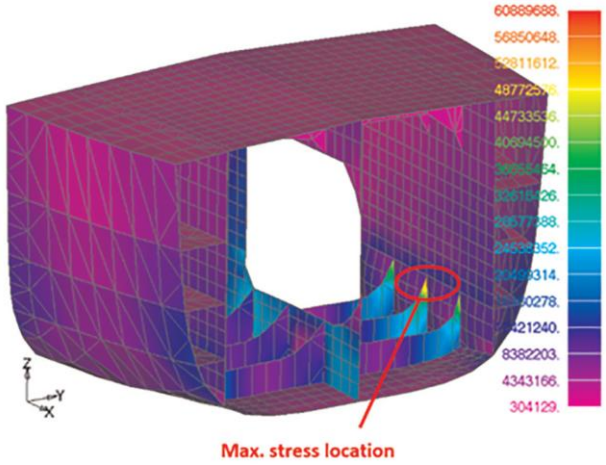

Fig. 2. Position of maximum von Mises stress [17].

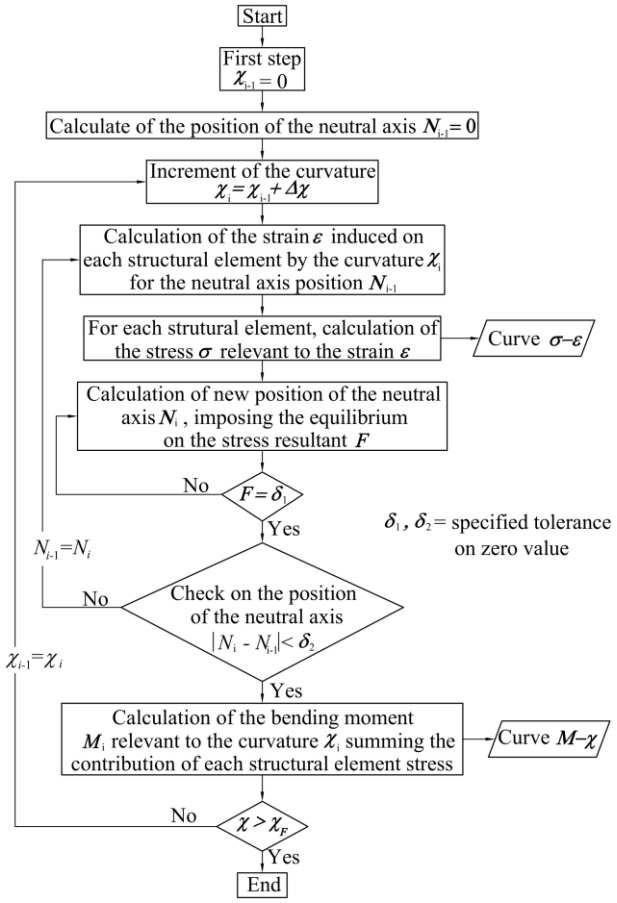

Fig. 3. Procedure for generating the M-χ curve.

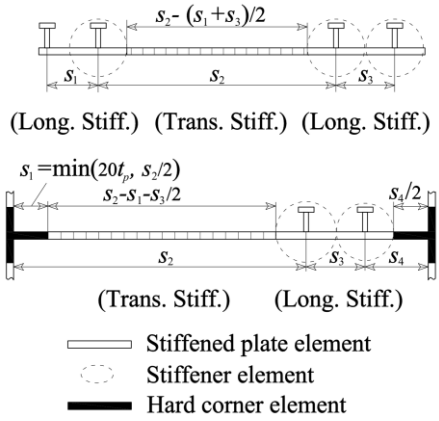

Fig. 4. Element classification.

evaluate compressive behavior considering plate and column slenderness and initial imperfections, proposing an empirical expression for predicting US. Ahmad et al. [11] investigated stiffened plates of floating production storage and offloading (FPSO) under axial loading through plating thickness and deformation. While most studies focus on steel structures, Wang et al. [12] analyzed aluminum stiffened panels, evaluating the effects of heat-affected zones (HAZ), welding patterns, panel dimensions, and combined biaxial compression and lateral pressure.

Regarding ship hull girders, stress-strain behavior has been examined across multiple ship types. For container ships, the ULS of bottom stiffened panels was analyzed using NFEA, incorporating effects of deflections, boundary conditions, corrosion, mesh size, and lateral pressure, with stress distribution (Fig. 1) and normalized stress-strain curves reported [13]. For warships, hull-girder responses to underwater explosions and wave-induced loads were assessed using acoustic structure interaction and NFEA, providing deformation patterns and strain curves [14]. For oil/chemical tankers, US performance of FPSOs under corrosion damage was evaluated through ultimate stresses of deck and outer-bottom stiffened panels under longitudinal and transverse compression and lateral pressure [15]. A full-scale double-hull tanker was analyzed using a single-layer equivalent model for intact, grounded, and collision-damaged conditions, covering deformation shapes under tension and compression [16]. A single-bottom oil tanker was studied for ULS under wave loads and towing forces [17], along with a reliability assessment considering cracking and pitting corrosion [18]. These studies provided von Mises stresses (Fig. 2) and average stress-strain curves for various structural components, including plating, bulkheads, shell structures, side tanks, bracket areas, and intact, pitted, cracked, and combined cracked-pitted plates.

Longitudinal structures in the midship region experience substantial stresses and strains under vertical bending moments. Evaluating these responses at the ULS is essential for determining the load-carrying and

Table 1. Modes of failure [19].

Element groups	Modes of failure
Stiffened plate element	Elasto-plastic collapse
Stiffener element	Beam column buckling
	Torsional buckling
	Web local buckling of flanged profiles
	Web local buckling of flat bars
Hard corner element	Plate buckling

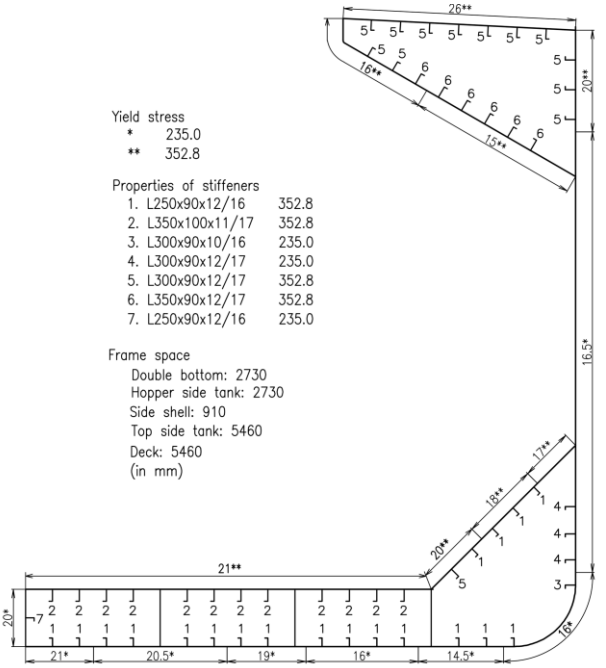

Fig. 5. Scantlings of cross-section.

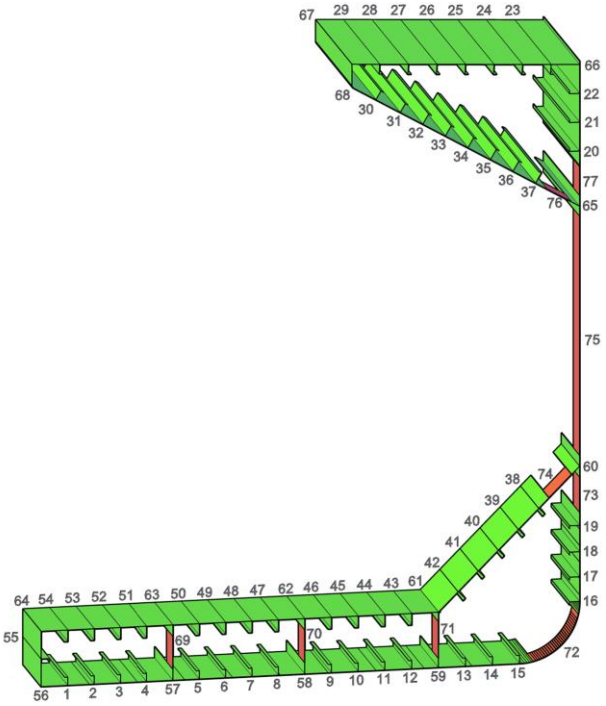

Fig. 6. Identification of structural element IDs.

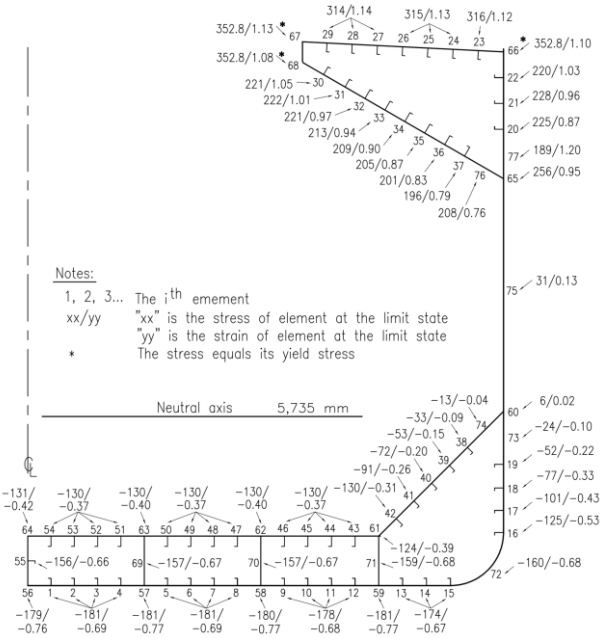

Fig. 7. Stresses and strains at the ULS for hogging condition.

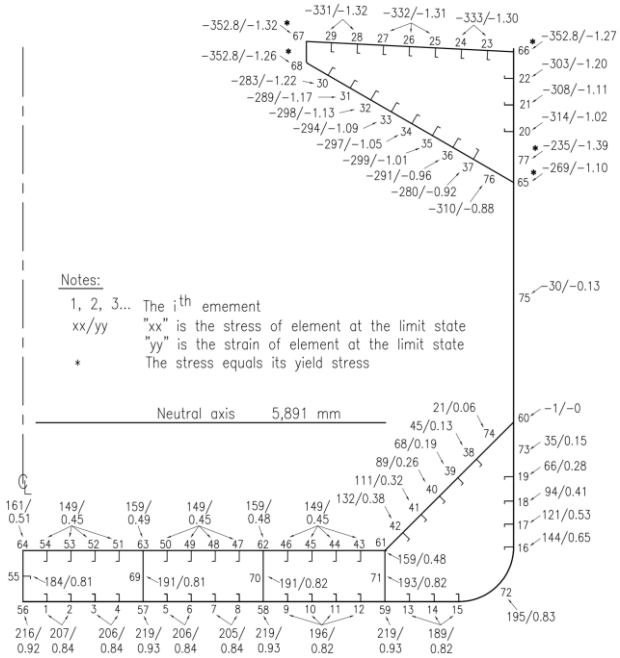

Fig. 8. Stresses and s trains at the ULS for sagging condition.

residual strength of individual structural elements, thereby supporting design adjustments for components susceptible to buckling or collapse under extreme loading. Previous studies have not addressed this issue in detail, particularly for BCs. Therefore, the present study concentrates on analyzing and evaluating the stress and strain of each longitudinal structural component in the cross-section of single-side BCs. Owing to their large dimensions, prominent hatch coamings, and single-side configuration, these vessels constitute a structurally critical ship type that continues to draw significant research attention.

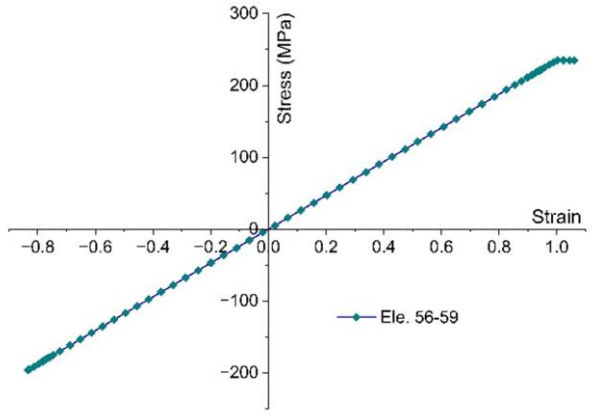

Fig. 9. Case of element IDs 56-59 (bottom region).

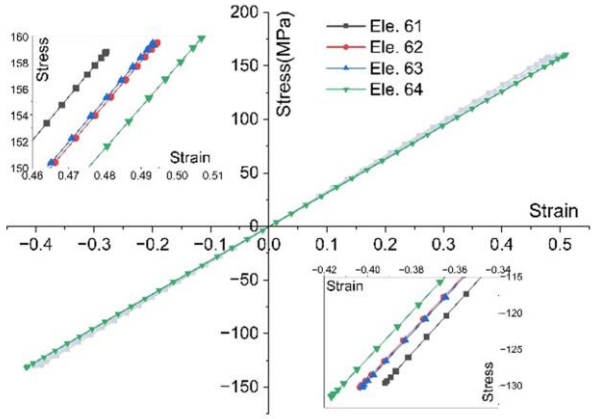

Fig. 10. Case of element IDs 61-64 (inner bottom region).

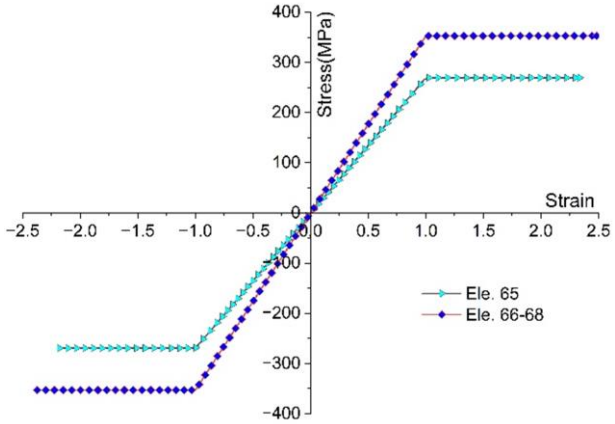

Fig. 11. Case of element IDs 65-68 (top-side tank and deck regions).

2. APPLICATION OF METHODS

2.1. Ultimate bending moments

The hull girder ULS is evaluated based on the ultimate bending moment (UBM). Various methods are available to determine the UBMs. Among them, the empirical formula-based approaches enable rapid estimation of the values of UBMs; however, they are limited in their ability to capture the stress and/or strain distribution across individual structural components.

Conversely, the NFEA method provides detailed insight into these parameters, but the calculation process is very resource-intensive and time-consuming; the convergence level and success of this method greatly depend on the experience of users and model setups. In light of these considerations, the present study employs the incremental-iterative method to simultaneously determine the UBMs and the variations of stress and/or strain of all structural elements within the cross-section. The selected method has been proposed in the rules of the IACS [19] and introduced in references [20, 21]. Figure 3 illustrates the procedure for generating the moment-curvature and stress-strain curves.

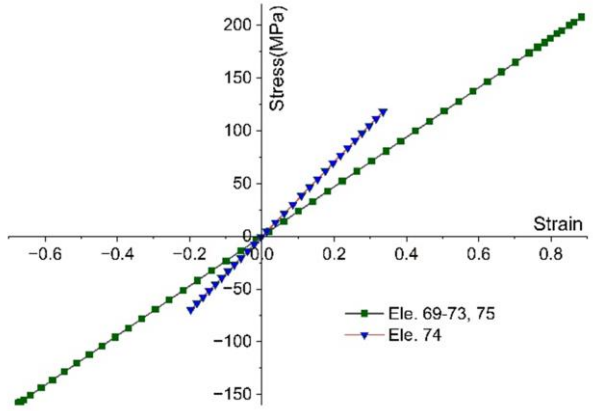

Fig. 12. Case of element IDs 69-75 (lengthened stiffened plate elements).

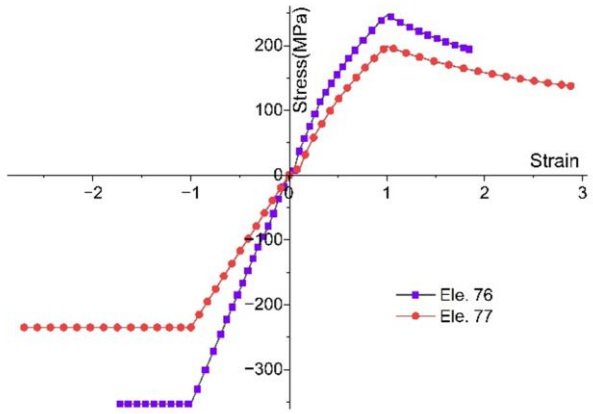

Fig. 13. Case of element IDs 76-77 (shortened stiffened plate elements, top-side tank region).

2.2. Stress and strain

To determine the stress and strain of each structural element, the subdivision of the hull cross-section into separate structural elements is a compulsory step for determining the stress and strain within each element. In accordance with the guidelines provided by the IACS, structural elements are categorized into three groups, as illustrated in Fig. 4. Each group of structural elements is assigned a specific mode of failure [19], as detailed in Table 1. These represent the typical failure modes of the stiffened plates.

When the ship hull is subjected to longitudinal bending, axial strain, ε, develops in the structural element,

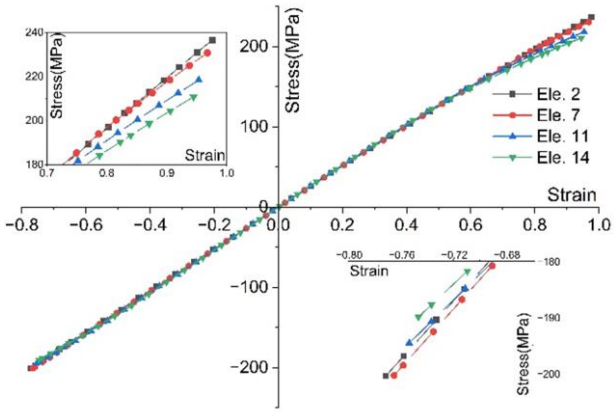

Fig. 14. Case of element IDs 2, 7, 11, and 14 (outer bottom region).

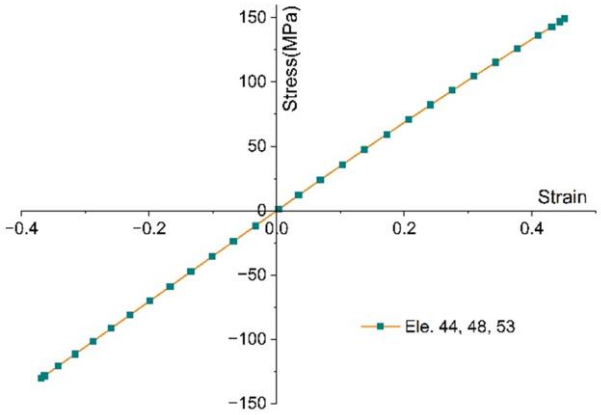

Fig. 15. Case of element IDs 44, 48, and 53 (inner bottom region).

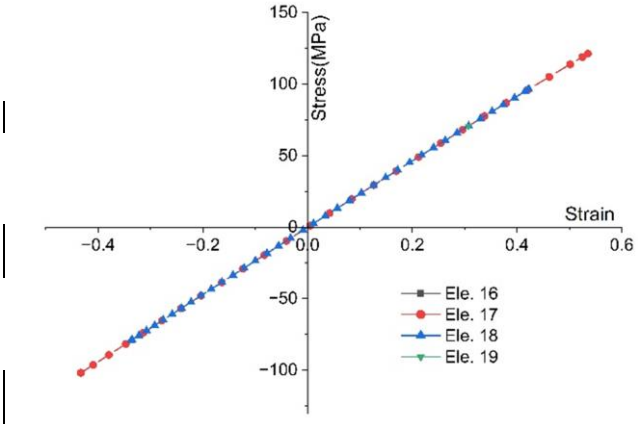

Fig. 16. Case of element IDs 16-19 (lower side region).

and its magnitude depends on the position of each element relative to the horizontal neutral axis. In the sagging condition, structural elements located below the neutral axis are lengthened, while the elements above the neutral axis are shortened; the opposite occurs in the hogging condition. The strain induces stress, σ, in each structural element, which are determined from the corresponding load-end shortening (σ-ε) curve of the element.

Table 2. Ship scantlings.

Items	Ship IDs			
	BC-1	BC-2	BC-3	BC-4
Δ, DWT	24,600	28,492	23,726	24,034
L_{OA}, m	157.22	169.26	150.52	153.5
L_{BP}, m	149.99	160.4	143.0	146.0
B, m	26.0	27.2	26.0	25.8
D, m	13.3	13.6	13.2	13.3
d, m	9.55	9.78	9.12	9.55

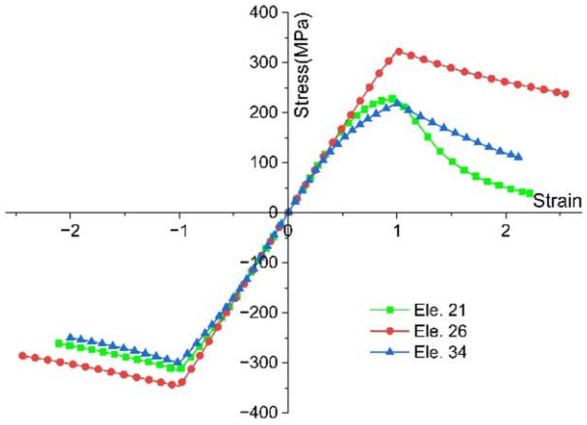

Fig. 17. Case of element IDs 21, 26, and 34 (top-side tank region).

The formulas describing the load-end shortening relationship for each structural element, corresponding to their assumed mode of failure, are presented as follows.

For elasto-plastic collapse, the load-end shortening relationship is expressed using formula (1), as shown below:

$$\sigma = \Phi R_{eHA} \quad (1)$$

For beam column buckling, the load-end shortening curve is determined based on formula (2), as presented below:

$$\sigma_{CR1} = \Phi \sigma_{C1} \frac{A_{s-n50} + A_{pE-n50}}{A_{s-n50} + A_{p-n50}} \quad (2)$$

For torsional buckling, the corresponding load-end shortening expression is derived from formula (3), as follows:

$$\sigma_{CR2} = \Phi \frac{A_{s-n50}\sigma_{C2} + A_{p-n50}\sigma_{CP}}{A_{s-n50} + A_{p-n50}} \quad (3)$$

For web local buckling of flanged profiles, the load-end shortening behavior is characterized using formula (4), as given below:

$$\sigma_{CR3} = \Phi \frac{10^3 b_E t_{n50} R_{eHp} + (h_w e t_{w-n50} + b_f t_{f-n50}) R_{eHs}}{10^3 s t_{n50} + h_w t_{w-n50} + b_f t_{f-n50}} \quad (4)$$

For web local buckling of flat bars, formula (5) provides the load-end shortening curve for this failure mode, as shown below:

$$\sigma_{CR4} = \Phi \frac{A_{s-n50}\sigma_{C4} + A_{p-n50}\sigma_{CP}}{A_{s-n50} + A_{p-n50}} \quad (5)$$

For Plate buckling, the load-end shortening response is described by formula (6), as presented below:

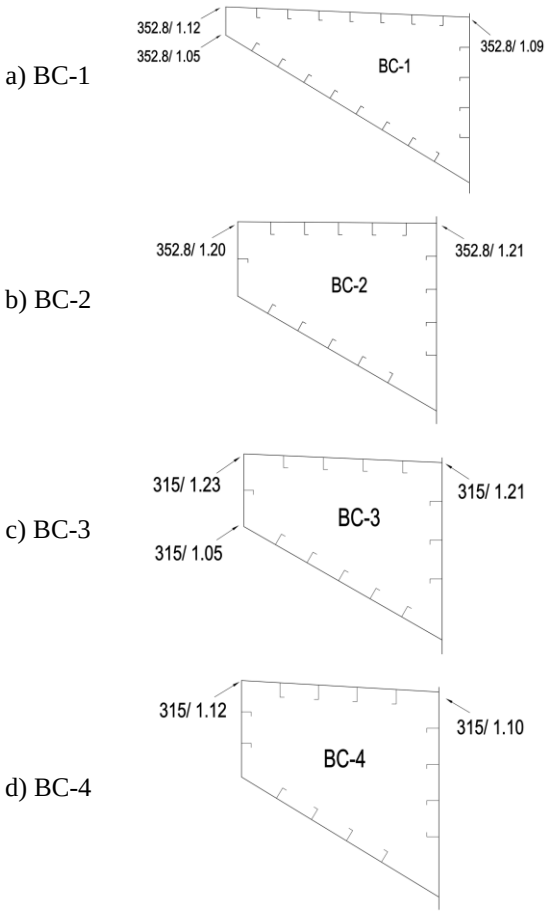

The notation "xx/yy" represents the stress (xx, MPa) and the strain (yy, dimensionless).

Fig. 18. The maximum stress in the hogging condition.

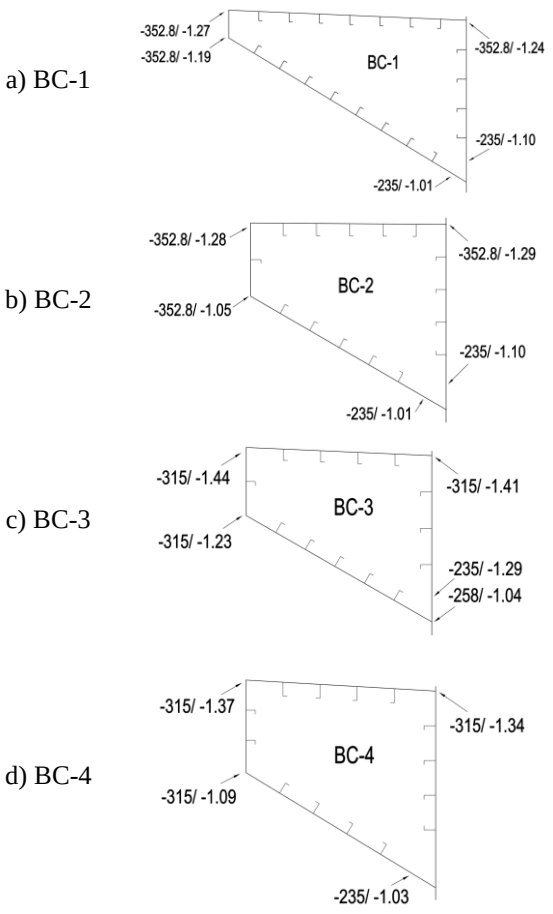

The notation "xx/yy" represents the stress (xx, MPa) and the strain (yy, dimensionless).

Fig. 19. The maximum stress in the sagging condition.

$$\sigma_{CR5} = \min\left\{\begin{matrix}\Phi R_{eHp} \\ \Phi R_{eHp}\left[\frac{s}{l}\left(\frac{2.25}{\beta_E}-\frac{1.25}{\beta_E^2}\right)+0.1\left(1-\frac{s}{l}\right)\left(1+\frac{1}{\beta_E^2}\right)^2\right]\end{matrix}\right. \quad (6)$$

The relative strain of each structural element is obtained by using formula (7), as follows [19]:

$$\epsilon = \frac{\epsilon_E}{\epsilon_Y} \quad (7)$$

where, R_{eHA} is equivalent minimum yield stress of the considered element, R_{eHs} is minimum yield stress of the material of the considered stiffener, R_{eHp} is minimum yield stress of the material of the considered plate, Φ is edge function, ε is relative strain, ε_E is element strain, ε_Y is strain at yield stress in the element, $A_{s\text{-}n50}$ is net sectional area without attached plating, $A_{p\text{-}n50}$ is net sectional area of attached plating, $A_{pE\text{-}n50}$ is net sectional area of attached plating of width b_E, t_{n50} is net offered thickness of the plate, b_E is effective width of the attached plating, h_{we} is effective height of the web, b_f is breadth of flange, $t_{f\text{-}n50}$ is the net thickness of flange, h_w is the height of web, $t_{w\text{-}n50}$ is the net thickness of web, σ_{C1}, σ_{C2}, and σ_{C4} are critical stresses, σ_{CP} is buckling stress of the attached plating, σ is the critical stress for case of elasto-plastic collapse, σ_{CR1} is the critical stress for case of beam column buckling, σ_{CR2} is the critical stress for case of torsional buckling, σ_{CR3} is the critical stress for case of web local buckling of flanged profiles, σ_{CR4} is the critical stress for case of web local buckling of flat bars, σ_{CR5} is the critical stress for case of plate buckling, s is spacing of the adjacent longitudinal stiffener, l is longer side of the plate, and β_E is the plate slenderless.

3. APPLICATION OF THE VESSEL

To illustrate the stress-strain relationships, a BC is utilized as a case study. The hull structure comprises a double-bottom, single-side, bilge hopper tanks, and top-side tanks. Figure 5 presents the mid-ship cross-section along with structure specifications, material properties, and frame spacing [21, 22]. The yield stress of the materials is 235.0 MPa for mild steel and 352.8 MPa for high-tensile steel. The plating thickness ranges from 14.5 mm to 26.0 mm. The longitudinal profiles consist of unequal angle types with web heights ranging from 250 mm to 350 mm. The distance between the two transverses in the double bottom and bilge hopper tank areas is 2,730 mm, whereas it is 5,460 mm in the deck and top-side tank areas. The frame spacing is 910 mm.

Figure 6 illustrates the shapes and identification of structural elements. As shown in Fig. 6, a total of 77 elements is classified into three groups. The group

comprising lengthened and shortened stiffened plate elements includes element IDs ranging from 69 to 77. The elements with IDs from 1 to 55 are categorized within the shortened stiffener element group. The hard corner element group includes elements with IDs ranging from 56 to 68.

4. RESULTS AND DISCUSSIONS

4.1. Stress and strain of structural elements

At the ULS corresponding to the UBMs, the stress and strain distributions of all structural elements within the cross-section of the selected vessel are presented in Figs. 7-8.

For hogging condition (Fig. 7), the side shell, deck, and top-side tank structures are located within the tension zone, whereas the double bottom and bilge hopper tank structures are situated within the compression zone. In the tension zone, the structural elements experience high stress levels, with several elements reaching the material's yield stress of 352.8 MPa, notably element IDs 66, 67, and 68, which correspond to hard corner elements. The maximum strain within this zone is recorded at 1.14, observed in element IDs 27, 28, and 29, which represent shortened stiffener elements within the deck panel. Conversely, in the compression zone located below the horizontal neutral axis, the compressive stresses in the structural elements remain significantly below the material's yield stress. The strain in this region reaches a maximum of -0.77, identified in element IDs 57, 58, and 59, corresponding to hard corner elements within the outer bottom panel.

For sagging condition (Fig. 8), the structural behavior exhibits a distribution opposite to that observed under the hogging condition. Specifically, the region above the neutral axis is subjected to compression, whereas the region below the neutral axis experiences tension. Within the compression zone, the structural elements exhibit high compressive stresses at the ULS, with several elements reaching the material's yield stress of 352.8 MPa, notably element IDs 65-68 and 77. The maximum strain in this zone is recorded at -1.32, observed in element IDs 28, 29, and 67. In the tension zone, the tensile stresses within most structural elements remain significantly below the material's yield stress. The maximum strain in this region is recorded at 0.93, occurring in the elements located farthest from the neutral axis, specifically element IDs 57, 58, and 59.

The stress-strain curves of varying structural elements are illustrated in Figs. 9-17.

4.2. Discussions

Several highlights can be discussed as follows:

(i) For hard corner elements: The stresses and strains of the hard corner elements (element IDs 56-68) were determined by using formulas (6) and (7). The stress-strain curves for these elements are illustrated in Figs. 9-11. Under the sagging condition, the hard corner elements located in the outer bottom region (element IDs 56-59) exhibit stresses that reach the material's yield stress of 235 MPa (Fig. 9). Similarly, the elements positioned farthest from the neutral axis (element IDs 65-68) approach the yield stress of 352.8 MPa (Fig. 11). The remaining hard corner elements display stress levels below the material's yield stress, with their stress-strain responses exhibiting linear behavior (Fig. 10).

(ii) For lengthened and shortened plate elements: The stresses in the lengthened and shortened stiffened plate elements are determined by using formulas (1) and (6), respectively, while the relevant strains are determined by using formula (7). At the ULS of vertical bending moments, the lengthened stiffened plate elements exhibit stress levels below the material's yield stress (Fig. 12). In contrast, under the sagging condition, the shortened stiffened plate elements reach the yield stress, whereas under the hogging condition, these elements attain their ultimate stress levels (Fig. 13).

(iii) For plate-stiffener combination elements: The stresses and strains of these elements are determined by using formulas (2)-(5) and (7), respectively. The stress-strain curves are presented in Figs. 14-17. As shown in Figs. 14-16, all structural elements located below the neutral axis exhibit stress levels below both the material's yield and ultimate stress values. In contrast, the structural elements located above the neutral axis reach their ultimate stress levels under both hogging and sagging conditions, as illustrated in Fig. 17.

(iv) Stress concentration: One noted feature observed from the Figs. 7 and 8 is that the structural elements within the top-side tank and strength deck exhibit the highest stress and strain under both sagging and hogging conditions. This behavior is explained by the considerable distance of these structures from the neutral axis. Under hogging and sagging conditions, the structures located above the neutral axis are subjected to tension and compression, respectively. At the ULS of the vertical bending moment, these structures experience significant strains, leading to elevated stress levels. Consequently, these stresses might reach the material's yield or ultimate stress values.

The other four BCs with similar characteristics in terms of dimensions, structural configuration, and geometry (Table 2) are used to illustrate the stress concentration within the top-side tank region. The results illustrating the maximum stress and strain for these vessels are presented in Figs. 18 and 19, corresponding to the hogging and sagging conditions, respectively.

Under the hogging condition, the maximum stresses reach the material's yield stress. These maximum stresses are observed at the intersections between the stringer plate and the sheer strake, as well as between the deck plating and the bottom slant plating of the top-side tank. For the BC-1 and BC-3 vessels, additional stress concentrations are identified at the intersection of the top-side tank longitudinal bulkhead plating and the bottom slant plating of the top-side tank (Fig. 18).

Under the sagging condition, the maximum stresses and strains are also observed at the same locations as identified under the hogging condition. In addition, the intersection between the side shell plating and the bottom slant plating of the top-side tank exhibits stress concentrations when the vessel reaches the ULS of the vertical bending moment (Fig. 19).

According to this result, the structural elements in the top-side tank region should be given special attention in the structural design, especially the elements with a

stress ratio at the ULS equal to the ultimate stress. This is also a recommendation from this study.

Based on these results, it is recommended that special attention be given to the structural elements within the top-side tank area during the design process, especially those elements exhibiting a stress equal to the material's ultimate stress. This consideration is emphasized as a key recommendation of the present study.

5. CONCLUSION

This paper has presented the scantling particulars of single-side BCs and a method for determining the UBMs, alongside the governing formulas for evaluating the stress-strain relationships of each group of structural elements. Comprehensive information regarding the stresses and strains of individual structural components at the mid-ship section of the selected vessels has been introduced, analyzed, and assessed from multiple perspectives. Based on these analyses, several conclusions can be drawn as follows:

(i) The stresses in the structural elements under the sagging condition are consistently higher than those observed under the hogging condition (Figs. 7 and 8).

(ii) For both sagging and hogging conditions, the stresses in the structural elements located above the neutral axis are significantly greater than those in the elements located below the neutral axis.

(iii) Different groups of structural elements exhibit different stress-strain relationships, including both linear and polynomial characteristics.

(iv) The stresses in various structural elements may reach either the material's yield stress or ultimate stress, depending on the type of applied loading (compressive or tensile).

(v) The strains at the ULS remain lower than the maximum strain capacity of each structural element.

(vi) The hard corner elements located in the top-side tank region attain the material's yield stress when the hull reaches the ULS of the vertical bending moment under both hogging and sagging conditions.

The insights obtained from this study contribute to a deeper understanding of the structural behavior of individual components within BC hull structures. The findings provide a basis for designers to refine and optimize structural elements that exhibit the highest stress and strain levels, thereby enhancing the longitudinal strength of the vessel, particularly at the ULS, and reducing the possibility of local failures that may lead to panel collapse or the entire hull structure collapse. Furthermore, the methodological approach and outcomes of this research can serve as a reference for the structural design and assessment of other merchant vessel types, including oil tankers, container ships, and roll-on/roll-off (RORO) vessels.

ACKNOWLEDGEMENT

This research is funded by Vietnam Maritime University under grant number: DT25-26.37.

REFERENCES

[1] S. Sultana et al., "Influence of corrosion on the ultimate compressive strength of steel plates and stiffened panels," *Thin-Walled Structures*, vol. 96, pp. 95–104, 2015.

[2] H. Huang, C. Jia, and L. Guo, "Effect of local corrosion on tensile behavior of steel plates," *Structures*, vol. 43, pp. 977–989, 2022.

[3] X. He and C. G. Soares, "Experimental and numerical study on the dynamic response of rectangular plates under repeated impacts," *Marine Structures*, vol. 96, pp. 103606, 2024.

[4] D. Shiomitsu et al., "A simple estimation method for ultimate strength of curved plates under axial compression," *The 42nd International Conference on Ocean, Offshore and Arctic Engineering, Vol. 2: Structures, Safety, and Reliability*, ASME, 2023.

[5] M. R. Khedmati, Z. H. M. E. Nouri, and K. Moradidohezari, "A computational investigation of the effects of both-sides general corrosion on the buckling/plastic collapse behavior and strength of stiffened plates," *Journal of Marine Science and Technology*, vol. 17, no. 1, pp. 68–93, 2011.

[6] D. K. Kim et al., "Effect of corrosion on the ultimate strength of double hull oil tankers - Part I: stiffened panels," *Structural Engineering and Mechanics*, vol. 42, no. 4, pp. 507–530, 2012.

[7] L. Feng et al., "A parametric study on effects of pitting corrosion on stiffened panels' ultimate strength," *International Journal of Naval Architecture and Ocean Engineering*, vol. 12, pp. 699–710, 2020.

[8] E. Hacihamud et al., "Non-linear buckling analysis of ship hull stiffened panels," *The 4th Conference of Computational Methods & Ocean Technology - IOP Conference Series: Materials Science and Engineering*, vol. 1294, IOP, 2023.

[9] M. Hanif et al., "Effect of design parameters on the ultimate strength and collapse behavior of stiffened panels," *Journal of Applied Engineering Science*, vol. 21, no. 3, pp. 940–956, 2023.

[10] D. K. Kim et al., "An empirical formulation for predicting the ultimate strength of stiffened panels subjected to longitudinal compression," *Ocean Engineering*, vol. 140, pp. 270–280, 2017.

[11] R. Ahmad, F. Husain, and M. Z. M. Alie, "Stiffened plate analysis by considering follow-up plates in the effect of one-way axial load on FPSO vessels," *Jurnal Inovasi Sains Dan Teknologi Kelautan*, vol. 4, no. 3, pp. 248–252, 2023.

[12] X. Wang, Z. L. Yu, and J. Amdahl, "Ultimate strength of welded aluminum stiffened panels under combined biaxial and lateral loads: A numerical investigation," *Marine Structures*, vol. 97, 103654, 2024.

[13] J. J. Cui, D. Y. Wang, and N. Ma, "A study of container ship structures' ultimate strength under corrosion effects," *Ocean Engineering*, vol. 130, pp. 454–470, 2017.

[14] H. C. Zhou et al., "Dynamic response of hull girder subjected to combined underwater explosion and wave-induced load," *Ocean Engineering*, vol. 235, 109436, 2021.

[15] D. K. Kim et al., "Time-dependent ultimate strength performance of corroded FPSOs," *Arabian Journal for Science and Engineering*, vol. 39, no. 11, pp. 7673–7690, 2014.

[16] T. Putranto, M. Kõrgesaar, and K. Tabri, "Application of equivalent single layer approach for ultimate strength analyses of ship hull girder," *Journal of Marine Science and Engineering*, vol. 10, no. 10, pp. 1–20, 2022.

[17] N. Vladimir et al., "Direct strength calculation of an aged single-bottom tanker during its towing in waves,"

Proceedings of the Institution of Mechanical Engineers -, Part M: *Journal of Engineering for the Maritime Environment*, pp. 1–14, 2023.

[18] F. Ahmadi, and A. R. Ranji, "Reliability assessment of ship hull girders considering pitting corrosion and crack," *Engineering Research Express*, vol. 6, no. 1, pp. 015503, 2024.

[19] IACS, "Common structural rules for bulk carriers and oil tankers," *International Association of Classification Societies*, 2024.

[20] V. T. Vu, and P. Yang, "Tool for predicting the ultimate bending moment of ship and ship-shaped hull girder," *Journal of Shanghai Jiao Tong University* (*Science*), vol. 23, no. 4, pp. 515–526, 2018.

[21] V. T. Vu, and D. T. Dong, "Hull girder ultimate strength assessment considering local corrosion," *Journal of Marine Science and Application*, vol.19, no.4, pp. 693–704, 2020.

[22] V. T. Vu, "Ultimate strength of aged ships under hull structure's imperfections," *International Conference on Marine Sustainable Development and Innovation - MSDI 2023, IOP Conference Series: Earth and Environmental Science*, vol. 1278, no. 1, IOP, 2023.